

Journal of Theoretical and Computational Chemistry
 Vol. 14, No. 7 (2015) 1550048 (22 pages)
 © World Scientific Publishing Company
 DOI: 10.1142/S0219633615500480



QM study of complexation between natural bilirubin and poly-terthiophene carboxylic acid-Mn(II) as a biosensor: Temperature and interferences effect

Mina Ghiasi^{*,‡}, Masoumeh Molaei^{*} and Mansour Zahedi[†]

**Department of Chemistry, Faculty of Science
 Alzahra University
 19835-389 Vanak, Tehran, Iran*

*†Department of Chemistry, Faculty of Science
 Shahid Beheshti University
 G. C. Evin, 19839-63113 Tehran, Iran
[‡]ghiasi@alzara.ac.ir*

Received 5 April 2015

Accepted 11 September 2015

Published

Bilirubin is an insoluble yellow pigment produced from heme catabolism and serves as a diagnostic marker of liver and blood disorders. Here, a systematic study of several interactions and arrangements between different forms of natural bilirubin and poly-5, 2'-5', 2''-terthiophene-3-carboxylic acid/Mn(II)₂ complex, PTTCA-Mn(II)₂, as a biosensor of bilirubin has been investigated extensively. The PTTCA-Mn(II)₂ biosensor detects natural bilirubin through the mediated electron transfer by the Mn²⁺. Initially, density functional theory (DFT) using B3LYP and different basis sets including 6-31G* and 6-311G** has been employed to calculate the details of electronic structure and electronic energies of natural biliverdin and δ -, β - and γ -bilirubin. Next, the interaction of the PTTCA-Mn(II)₂ biosensor, being in three possible spin states, with δ -, β - and γ -natural bilirubin with 1:1 and 1:2 stoichiometry using UB3LYP/6-31G* method has been investigated. Natural population analysis (NPA) calculations have been used to derive more suitable interaction sites of bilirubin with Mn²⁺ ions in PTTCA-Mn(II)₂ biosensor. Investigation of different manganese complexes with bilirubin shows that the most stable complex is high spin state (total electron spin $S = 5/2$) rather than intermediate and low spin states with 1:2 stoichiometry. Also, the temperature effect and interferences from other biological compounds such as ascorbic acid, L-glutamic acid, uric acid, creatine, glucose and dopamine have been investigated. The nature of the interaction between manganese metal cations and natural bilirubin is also discussed employing NPA, molecular orbital (MO) analysis and Bader's Atoms in Molecule (AIM) theory.

Keywords: Bilirubin; polyTTCA-Mn(II)₂ complex; biosensor; QM calculation.

[‡]Corresponding author.

M. Ghiasi, M. Molaei & M. Zahedi

1. Introduction

Bilirubin is cytotoxic yellow pigment of jaundice, produced by catabolism of heme and other iron porphyrin containing enzymes in mammals, and presents in the blood as an unconjugated (free) form. Biliverdin can be reduced chemically to bilirubin from three positions δ , β and γ as shown in Fig. 1, but in the presence of bilirubin reductase enzyme just γ -bilirubin is formed.^{1–5} Many experimental and theoretical studies have shown the rigid-tilde conformation for natural bilirubin,^{6–10} bilirubin dianion¹¹ and octa ethyl bilirubin as a model compound of bilirubin.¹² The path of reduction of the biliverdin to bilirubin was studied theoretically using the semiempirical methods which confirmed the production of γ -biulirubin as the most stable form of bilirubin isomers.⁵ This path has also been clarified by a model of bilirubin, octa ethyl bilirubin, using experimental and computational methods.¹²

In addition, determination of bilirubin in blood serum is considered as a true test of liver function in medicine.^{13,14} Since bilirubin is a toxic compound, an excess amount of bilirubin in serume from its normal level, 1.93–3 mg/dl, in humans is associated with liver disease, such as cirrhosis or hepatitis, jaundice and in addition damage of central nervous system or even death especially in newborn babies.^{15–18}

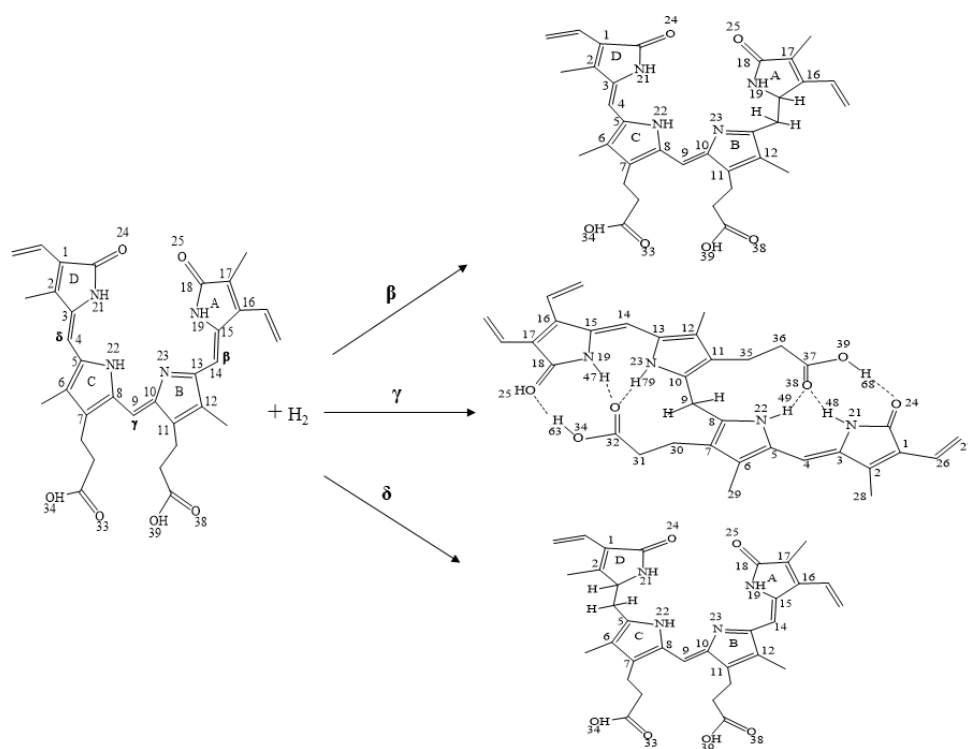


Fig. 1. Schematic representation of reduction paths of natural biliverdin from three meso carbon positions δ , γ , and β with numbering for key atoms.

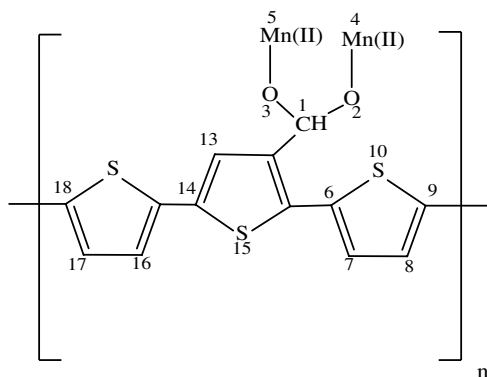


Fig. 2. Presentation of (polyTTCA)/Mn(II)₂ complex structure with numbering system included.

Therefore, the correct determination of bilirubin is very important and there are several methods for detection of bilirubin in clinical samples.^{19–26}

Rahman *et al.*²⁷ have proposed an amperometric bilirubin biosensor fabricated by complexing the Mn(II) ion with a conducting polymer, poly-5,2'-5',2''-terthiophene-3-carboxylic acid (PTTCA) as shown in Fig. 2. Each terthiophene monomer in the PTTCA-Mn(II) structure bears a carboxylic acid group, 5,20-50,200-terthiophene-3-carboxylic acid (TTCA). The final structure of the biosensor was fabricated by complexing Mn(II) ion with polyTTCA film. As Fig. 2 shows, each monomer of this biosensor has two Mn²⁺ ions which can interact with the bilirubin molecules.

The PTTCA–Mn(II)₂ complex biosensor exhibited good stability and fast response time and was tested in a human serum sample. However, the details of electronic structures, energy stabilities and interaction sites between bilirubin and this biosensor have not been identified yet. Wide dynamic range, short response time, low detection limit, and long lifetime stability are the advantages of this proposed bilirubin biosensor.

Besides large amount of studies, bilirubin still attracts the attention of scientists because of several chemical and biological properties. Therefore, in the present work we study the chemical reduction of natural biliverdin to bilirubin in the presence of solvent. Complexation of different forms of bilirubin and PTTCA–Mn(II)₂ biosensor has been studied with different stoichiometries and different multiplicities extensively. Full understanding of the role played by the manganese ion requires detailed knowledge of the interaction modes and energies of Mn(II) with natural bilirubin, the knowledge that is far from complete. So, we decided to analyze the details of structural, partial charges, and energetic components of the process of molecular recognition of bilirubin by PTTCA–Mn(II)₂ complex.

2. Computational Methods

Quantum mechanical calculations were carried out with the Gaussian program series 2003.²⁸ The geometries of natural biliverdin and different forms of natural bilirubin

M. Ghiasi, M. Molaei & M. Zahedi

were fully optimized employing a hybrid Hartree–Fock density functional scheme, the adiabatic connection method, Becke three-parameter with Lee–Yang–Parr (B3LYP) functional^{29–31} of density functional theory (DFT)³⁰ with the standard 6-31G^{*32} and 6-311G^{**33} basis sets. For the PTTCA–Mn(II)₂ complex and different complexes between different forms of bilirubin and PTTCA–Mn(II)₂ complex, calculations were made with the unrestricted formalism, UB3LYP, using 6-31G^{*} basis set. All full optimizations were performed without any symmetry constraints. The harmonic vibrational frequencies were computed to confirm that an optimized geometry correctly corresponds to a local minimum that has only real frequencies. Net atomic charges and spin densities were obtained using natural population analysis (NPA) of Frisch *et al.*³⁴ The solvent effect on the conformational equilibrium was investigated with polarized continuum model (PCM).³¹ Solvation calculations were carried out for water with geometry optimizations for this solvent. A topological analysis, describing the nature of the interactions, was performed to calculate the charge density (ρ) and its second derivative, Laplacian of charge density ($\nabla^2\rho$), for bonds using Bader’s Atoms in Molecule (AIM) theory.³⁵

3. Results and Discussion

3.1. Geometry optimization of natural biliverdin molecule and its reduced forms

As a starting point, the structure of natural biliverdin was drawn and fully optimized at B3LYP method using 6-31G^{*} and 6-311G^{**} basis sets with no initial symmetry restrictions and assuming C_1 point group. According to Fig. 1, reduction process of natural biliverdin was carried out by letting a hydrogen molecule approach to meso carbon from δ , γ and β positions each time separately. The optimized geometry of biliverdin and reduced forms in the gas phase reoptimized by considering the solvent effect ($\epsilon = 78.9$) using PCM method.³¹ The structural details of optimized structures of biliverdin and three isomers of bilirubin are presented in Table 1. Comparison of reaction energies between different forms of bilirubin indicates that δ and β have similar energy and γ -bilirubin is the most stable form of bilirubin isomers by about 28 kcal/mol and 21 kcal/mol in gas phase and solution phase, respectively, by using B3LYP/6-31G^{*} and B3LYP/6-311G^{**} methods, see Table 2. Also, to show the stability of different forms of bilirubin in the presence of the water molecules, 11 water molecules were added to different optimized isomers of bilirubin at different positions that have potential to form hydrogen bonding with solvent molecules. The results of calculations indicate that the stability of γ -bilirubin in the presence of 11 water molecules reduce to 8.3 kcal/mol rather than 20 kcal/mol using PCM method; however, γ -bilirubin in Fig. 3(b) is the most stable form of isomer of bilirubin rather than β and δ -bilirubin.

The negative value of calculated reaction’s energy change, $\Delta E_{\text{rxn}} = E_{\text{bilirubin}} - (E_{\text{biliverdin}} + E_{\text{H}_2})$ indicates that the reduction of natural biliverdin to bilirubin is

QM study of complexation between natural bilirubin and PTTCA-Mn(II)

Table 1. Presentation of some chemical structural details of optimized biliverdin and different forms of bilirubin in gas and solution phase (in the parenthesis), respectively.

Connected atoms	β -bilirubin	δ -bilirubin	biliverdin
Bond distance (Å)			
C9–C10	1.38 (1.38)	1.38 (1.38)	1.38 (1.38)
C3–C4	1.37 (1.37)	1.56 (1.56)	1.37 (1.37)
C14–C15	1.56 (1.56)	1.36 (1.36)	1.36 (1.36)
C3–N21	1.40 (1.40)	1.45 (1.45)	1.40 (1.40)
C15–N19	1.45 (1.45)	1.38 (1.38)	1.39 (1.39)
Bond angle (°)			
C8–C9–C10	126.91 (126.92)	126.88 (126.88)	124.15 (124.15)
C3–C4–C5	129.50 (129.50)	115.25 (115.25)	128.64 (128.64)
C13–C14–C15	111.51 (111.51)	124.93 (124.93)	133.96 (133.96)
C4–C3–N21	126.19 (126.19)	113.05 (113.05)	127.46 (127.46)
C14–C15–N19	110.90 (110.90)	123.03 (123.03)	119.61 (119.61)
C9–C10–N23	121.81 (121.81)	123.68 (123.68)	122.01 (122.01)
Dihedral angle (°)			
C11–C10–C9–C8	−178.85 (−178.85)	177.71 (177.71)	−178.47 (−178.47)
C10–C9–C8–C7	−178.61 (−178.62)	174.14 (174.14)	−175.29 (−175.29)
C12–C13–C14–C15	−98.40 (−98.40)	172.38 (172.38)	−47.67 (−47.67)

energetically favorable in both gas and solution phases. Stabilization of the γ -biilirubin ridge-tile conformation is the result of six intramolecular hydrogen bonds that were first detected by X-ray crystallography.^{11,12} The difference in the heavy atom distances between X-ray data and the calculated value at B2PLYPD/6-31G* level of theory is rechecked, Table 3, which is in good agreement with the above mentioned methods. The optimized structures of biliverdin in solvent phase, using PCM method, and γ -biilirubin, using both PCM and explicit solvent methods, have been depicted in Fig. 3. To compare the results with experimental data, the most stable conformer of bilirubin, γ -biilirubin, has been reoptimized with B3LYP/6-311++G** method. Comparison between six predicted hydrogen bond distances with theoretical calculation and X-ray data, Table 3, indicates that the standard deviation for the 6-31G*, 6-311G** and 6-311++G** basis sets are 0.67, 0.71 and 0.39, respectively, so all methods corroborate well with experimental data. Our results are also in good agreement with previous results by Zahedi *et al.*⁵ The

Table 2. Comparison of reduction energies related to process of natural biliverdin reduction to different forms of bilirubin in gas and solution phases by using different methods.

Isomer	$\Delta E_{\text{rxn.}}$ (kcal.mol ^{−1}) (gas)		$\Delta E_{\text{rxn.}}$ (kcal.mol ^{−1}) (solvent)	
	B3LYP/6-31G*	B3LYP/6-311G**	B3LYP/6-31G*	B3LYP/6-311G**
β -Bilirubin	−28.67	−27.98	−29.09	−31.22
γ -Bilirubin	−56.94	−55.34	−50.62	−52.17
δ -Bilirubin	−28.83	−27.61	−29.26	−30.25

M. Ghiasi, M. Molaei & M. Zahedi

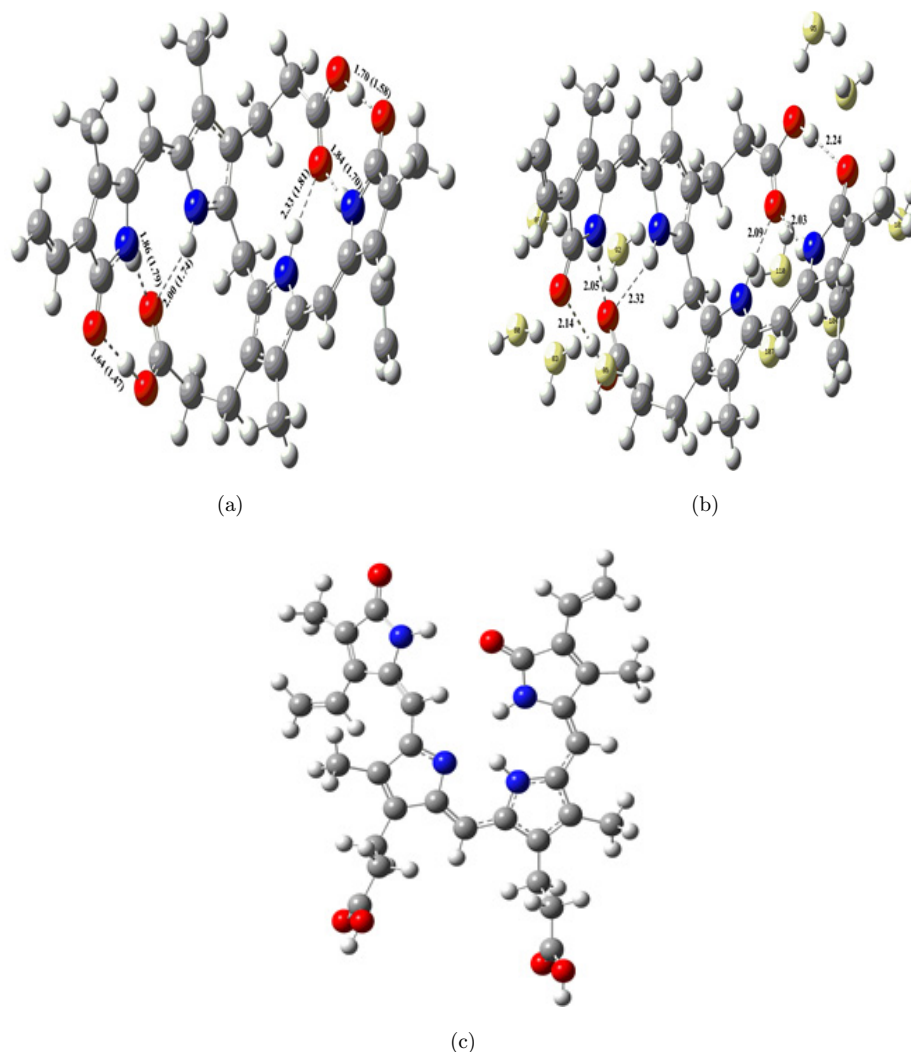


Fig. 3. Optimized structures of natural γ -bilirubin in the gas phase and solvent phase, using PCM method, (a) γ -bilirubin in the presence of explicit water molecules, (b) in natural biliverdin, and (c) in water solvent; the hydrogen bonding distances (Å) in γ -bilirubin molecule are presented in the gas phase and solvent phase, in parenthesis using PCM method.

adequacy of density functional methods with 6-31G* basis set to study the interaction between manganese and different compounds has been subject of several papers.^{36,37} Therefore, to reduce the computational cost, B3LYP method with 6-31G* basis set was applied to optimize the different PTTCA-Mn(II)₂/bilirubin complexes.

Calculation of vibrational frequencies has confirmed stationary point with no negative eigenvalue observed in the force constant matrix.

QM study of complexation between natural bilirubin and PTTCA-Mn(II)

Table 3. Comparison of calculated hydrogen bonds and heavy atom distances in γ -bilirubin in gas phase with X-ray data and the results of semi empirical methods studied in Ref. 5.

System	X-ray	B3LYP/ 6-31G*	B3LYP/ 6-311G**	B3LYP/ 6-11++G**	B2PLYPD/ 6-31G*	AM1, Ref. 5
Heavy atom distance						
N21-O38	2.75	2.82	2.82	2.61	2.82	2.95
O25-O34	2.55	2.65	2.62	2.60	2.65	3.20
N19-O33	2.83	2.84	2.84	2.83	2.84	3.06
N23-O33	2.80	2.95	2.97	2.82	2.96	2.97
Hydrogen bond distance						
H68...O24	1.58	1.70	1.69	1.61	1.71	2.10
H48...O38	1.70	1.84	1.85	1.80	1.85	2.13
H49...O38	1.81	2.33	2.38	2.00	2.33	2.15
H63...O25	1.47	1.64	1.62	1.63	1.64	2.20
H47...O33	1.79	1.86	1.86	1.80	1.86	2.21
H79...O33	1.74	2.00	2.02	1.98	2.01	2.24
Standard deviation		0.67	0.71	0.39	0.68	1.44

3.2. Optimization of PTTCA-Mn(II)₂ complex

The PTTCA-Mn(II)₂ complex involves two manganese cations which has an open shell system with a 3d⁵ ground state configuration.³⁸ So, several possible electronic states are coming from the different occupations of the 3d orbitals. Therefore, PTTCA-Mn(II)₂ complex was fully optimized at UB3LYP method using 6-31G* basis set with no initial symmetry restrictions and assuming *C*₁ point group at the low spin (*S* = 1/2), intermediate (*S* = 3/2) and high spin state (*S* = 5/2) multiplicities in the gas phase and in the presence of five water molecules, hydrated PTTCA-Mn(II)₂, PTTCA/Mn(II)₂(H₂O)₁₀, which provide an octahedral structure for each Mn(II) cation. Figure 4 demonstrates the optimized geometry of the monomer of the PTTCA/Mn(II)₂(H₂O)₁₀ in different spin states as well as relative energy stabilization. As the results show, high spin state is about 104.31 and 93.42 kcal/mol more stable than low and intermediate spin states for this complex, respectively.

To provide some analysis on why the high spin state shown in Fig. 4 is much lower in energy than the other spin states, the NPA calculation to find spin densities and partial charges has been carried out, see Table 4. As the results show, the numerical values of spin densities and particle charges on both Mn²⁺ cation and connected atom to Mn²⁺ in the high spin state are closer than other states. Therefore, this distribution of charges and spin densities lead to more stability of high spin state rather than low and intermediate spin states.

3.3. Details of atomic net charge

To find more suitable atomic sites of natural bilirubin to interact with both manganese cations in PTTCA-Mn(II)₂ biosensor, the net atomic charges on different

M. Ghiasi, M. Molaei & M. Zahedi

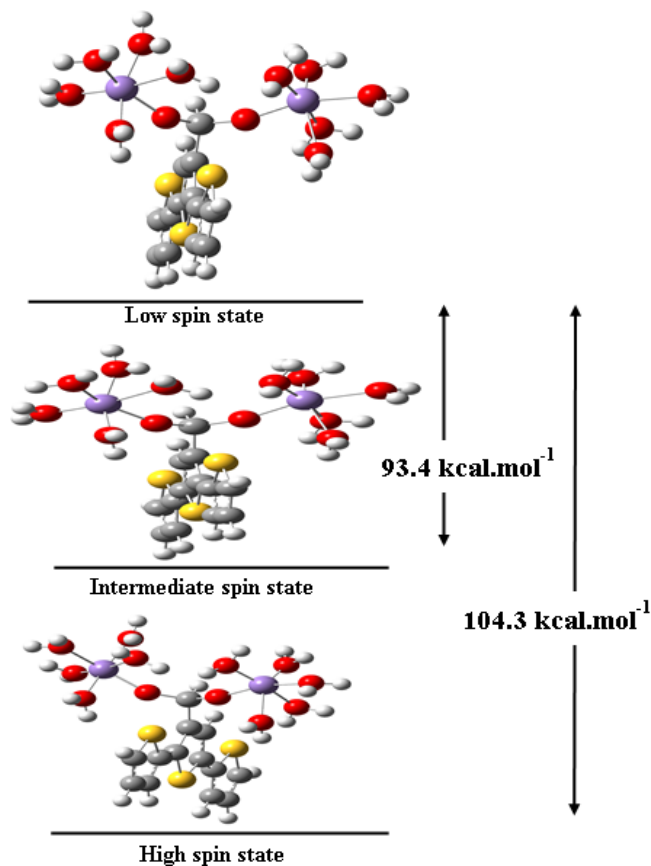


Fig. 4. Computed relative energy for optimized structure of the monomer of PTTCA/Mn(II)₂(H₂O)₁₀ biosensor at the different spin states in the water solvent.

forms of bilirubin are evaluated and presented in Table 5. These partial charges are derived from NPA calculation. The more negative charges have been detected on the nitrogen and oxygen atoms in three forms of bilirubin. In conclusion, these atoms are more preferred than other atoms to interact with manganese cations.

Table 4. Calculated net atomic charges and spin densities in PTTCA–Mn(II)₂ complex in different spin states.

Atom number	Spin density			Charge		
	11	7	3	11	7	3
Mn(4)	4.88	1.12	3.02	1.44	1.37	1.36
Mn(5)	4.88	4.88	−0.96	1.44	1.43	1.38
O(2)	0.09	−0.11	−0.03	−0.69	−0.65	−0.63
O(3)	0.09	0.09	−0.03	−0.69	−0.68	−0.66
C(1)	0.01	0.02	0.00	0.32	0.32	0.32

QM study of complexation between natural bilirubin and PTTCA-Mn(II)

Table 5. Computed net atomic charges on selected atoms in δ , β and γ -bilirubin.

Atom number	Particle atomic charges		
	γ -bilirubin	β -bilirubin	δ -bilirubin
N(21)	−0.80	−0.76	−0.64
N(22)	−0.71	−0.77	−0.73
N(23)	−0.74	−0.62	−0.72
N(19)	−0.79	−0.60	−0.74
O(24)	−0.59	−0.51	−0.53
O(25)	−0.60	−0.57	−0.54
O(33)	−0.53	−0.46	−0.46
O(34)	−0.58	−0.57	−0.56
O(38)	−0.52	−0.46	−0.47
O(39)	−0.59	−0.57	−0.58
C(1)	−0.11	0.02	0.06
C(9)	−0.43	−0.26	−0.25
C(14)	−0.25	−0.34	−0.28
C(15)	0.35	−0.04	−0.35
C(26)	−0.36	−0.11	0.11
C(28)	−0.55	−0.55	−0.57
C(29)	−0.54	−0.54	−0.55
C(30)	−0.35	−0.36	−0.36
C(35)	−0.36	−0.36	−0.36
C(36)	−0.34	−0.35	−0.37
C(40)	−0.54	−0.54	−0.54

3.4. Interaction study between PTTCA-Mn(II) complex, PTTCA-Mn(II)₂ and natural bilirubin

After optimizing various isolated isomers of bilirubin and PTTCA-Mn(II)₂ biosensor, we turned our attention to the complex formation between bilirubin and PTTCA-Mn(II)₂ biosensor to form different PTTCA-Mn(II)₂/bilirubin complexes. The main goal of our approach has been to study the arrangements that occur when bilirubin comes as close as possible to the two Mn²⁺ ions of biosensor moiety. Calculation of net charge over the different PTTCA-Mn(II)₂/bilirubin complexes and especially manganese ion has been carried out subsequently.

One would naturally expect bonding from electron rich atoms with high donor capability, such as nitrogen and carbonyl oxygen in bilirubin, to be of high importance to interact with manganese cation in biosensor. Also, two different combinations between Mn²⁺ ions and different isomers of bilirubin molecule are possible: (a) complexation of one monomer of the biosensor molecule with two bilirubin molecules (1:2 stoichiometry) and (b) complexation of one monomer of the biosensor molecule with one bilirubin molecule (1:1 stoichiometry). It is noticeable that for each complexes three different spin states are possible.

According to calculated results, for δ and β -bilirubin isomers just 1:2 stoichiometry, [PTTCA-Mn(II)₂/(δ -bilirubin)₂]⁴⁺ and [PTTCA-Mn(II)₂/(β -bilirubin)₂]⁴⁺ complexes will be formed.

M. Ghiasi, M. Molaei & M. Zahedi

Table 6. Presentation of some structural details of [PTTCA–Mn(II)₂/(δ -bilirubin)₂]⁴⁺, and [PTTCA–Mn(II)₂/(δ -bilirubin)₂(H₂O)₂]⁴⁺ complexes in high spin states.

Connected atoms	[PTTCA–Mn(II)/ (δ -bilirubin) ₂ (H ₂ O) ₂] ⁴⁺	[PTTCA–Mn(II)/ (δ -bilirubin) ₂] ⁴⁺
Bond distance (Å)		
Mn4–O2	1.99	2.06
Mn4–O64	2.10	—
Mn4–N26	2.30	2.34
Mn4–N27	2.21	2.16
Mn4–N28	2.31	2.30
Bond angle (°)		
O2–Mn4–O64	97.00	—
O2–Mn4–N26	125.37	96.67
O2–Mn4–N27	118.51	168.2
O3–Mn5–O65	93.75	—
O3–Mn5–N26'	101.23	112.29
O3–Mn5–N27'	101.25	114.08
Dihedral angle (°)		
C1–O2–Mn4–N27	169.17	166.91
C1–O3–Mn5–N27'	158.62	–126.03

The geometry of [PTTCA–Mn(II)₂/(δ -bilirubin)₂]⁴⁺ and [PTTCA–Mn(II)₂/(β -bilirubin)₂]⁴⁺ complexes have been optimized in low ($S = 1/2$), intermediate ($S = 3/2$) and high ($S = 5/2$) spin states. Our results show that the high spin state is about 24.45 kcal/mol and 17.51 kcal/mol more stable than low and intermediate spin states for both complexes. Some structural details of [PTTCA–Mn(II)₂/(δ -bilirubin)₂]⁴⁺ in high spin states are compiled in Table 6 according to the numbering of the system as shown in Fig. 5. The [PTTCA–Mn(II)₂/(δ -bilirubin)₂]⁴⁺ and [PTTCA–Mn(II)₂/(β -bilirubin)₂]⁴⁺ complex structures indicate that the coordination number of manganese cation is five and these complexes have square pyramid geometry, see Fig. 5 and Table 6. The interaction sites of δ - and β -bilirubin are N26, N27, N28, and O2 (or O3) atoms.

Therefore, in the next step the water molecule coordinates to each manganese cation for all complexes at the three different spin states, providing a six coordinated complex. Relative stability energy calculations for mentioned complexes, [PTTCA–Mn(II)₂/(δ -bilirubin)₂(H₂O)₂]⁴⁺ and [PTTCA–Mn(II)₂/(β -bilirubin)₂(H₂O)₂]⁴⁺, indicate that the high spin state is about 17 kcal/mol and 12 kcal/mol more stable than low and intermediate spin states, respectively, for both complexes. Figure 5 demonstrates computed energy stabilization and optimized geometries of five and six coordinates in high spin state for [PTTCA–Mn(II)₂/(δ -bilirubin)₂]⁴⁺ and [PTTCA–Mn(II)₂/(δ -bilirubin)₂(H₂O)₂]⁴⁺ complexes. As depicted in Fig. 5, the six-coordinated complex is about 35.72 kcal/mol more stable than five-coordinated complex in high spin state for δ - and β -bilirubin. Some structural details of [PTTCA–Mn(II)₂/(δ -bilirubin)₂(H₂O)₂]⁴⁺ complex have been shown in Table 6.

QM study of complexation between natural bilirubin and PTTCA-Mn(II)

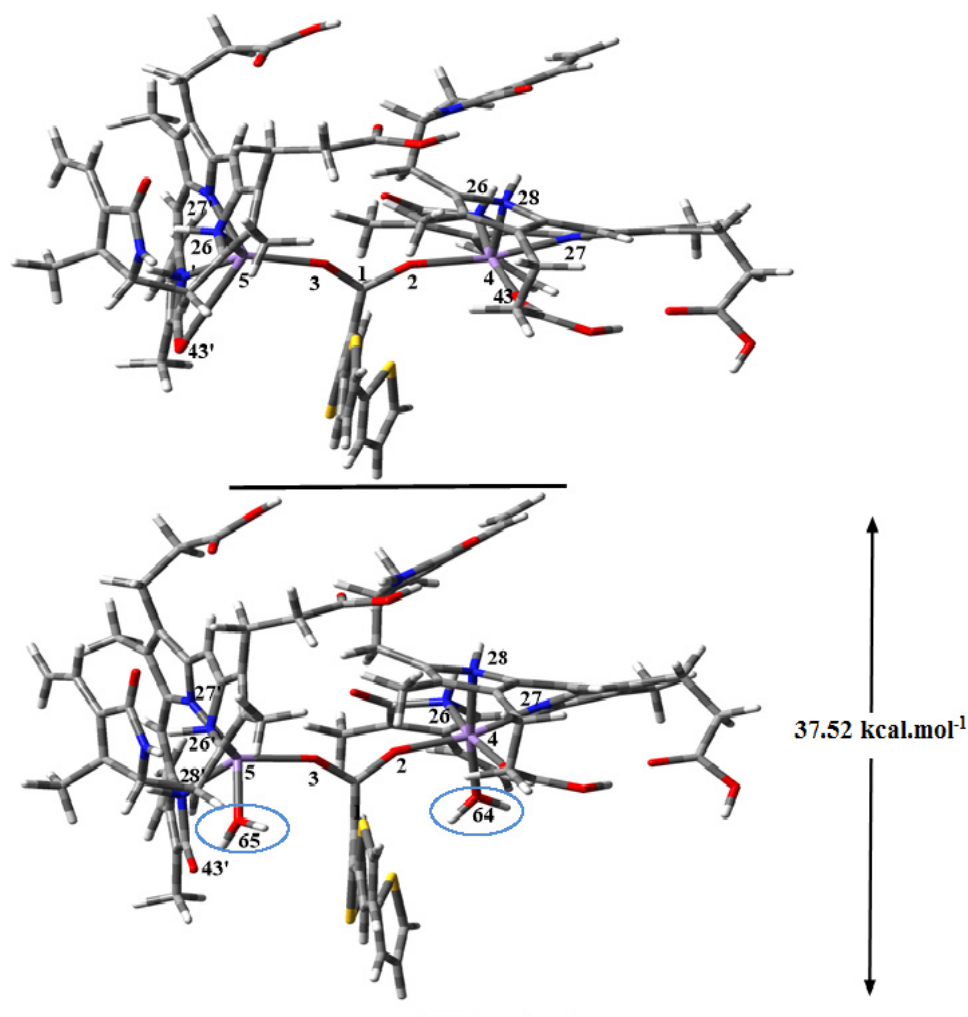


Fig. 5. Computed relative energy for optimized structure of $[\text{PTTCA-Mn(II)}_2/(\delta\text{-bilirubin})_2]^{4+}$ (up) and $[\text{PTTCA-Mn(II)}_2/(\delta\text{-bilirubin})_2(\text{H}_2\text{O})_2]^{4+}$ (down) complexes in high spin states with numbering for some key atoms, the position of water molecules has been defined with circle.

In the next step, we focused on the γ -bilirubin, the most stable isomer of bilirubin. At first, $[\text{PTTCA-Mn(II)}_2/\gamma\text{-bilirubin}]^{4+}$ complex (1:1 stoichiometry) has been fully optimized at the three different spin states. As the calculated results indicate, both Mn^{2+} cations in the biosensor molecule have four-coordinate with tetrahedral geometry and high spin state is about 128 kcal/mol and 240 kcal/mol more stable than intermediate and low spin states, respectively. Figure 6 (top) presents the optimized geometry of $[\text{PTTCA-Mn(II)}_2/(\gamma\text{-bilirubin})]^{4+}$ complex in high spin state. The coordinated sites of γ -bilirubin to the Mn4 atom are N26, N27, O43, and O2 and to the Mn5 are N24, N28, O38, and O3 atoms, respectively. The second possible

M. Ghiasi, M. Molaei & M. Zahedi

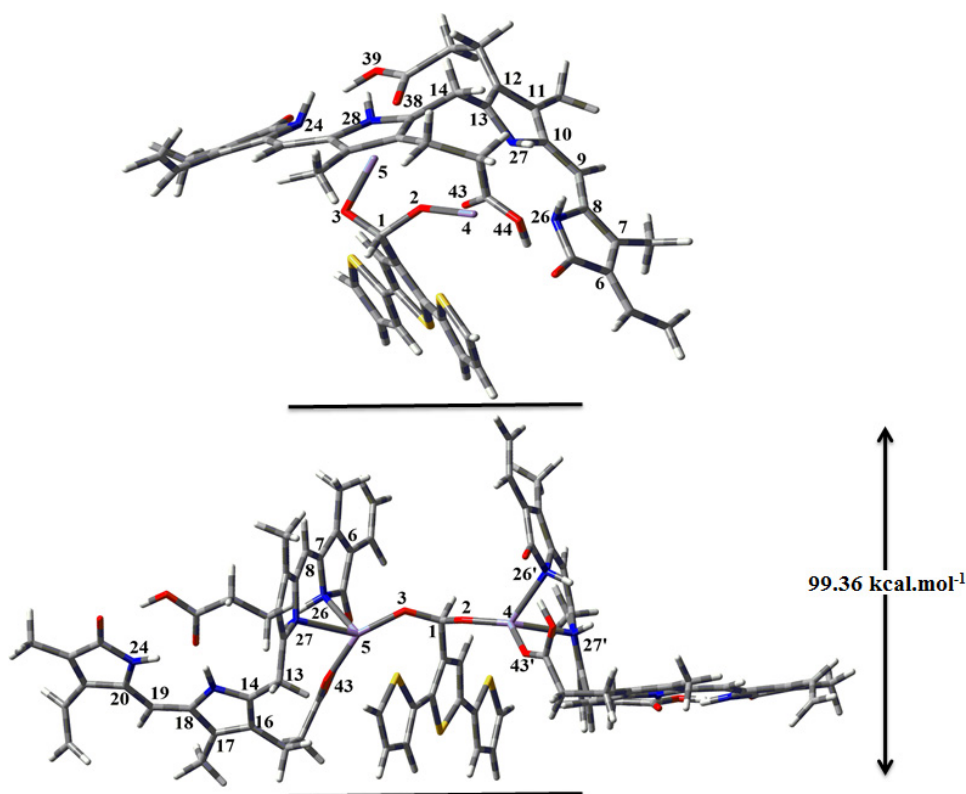


Fig. 6. Comparison of relative energy between $[\text{PTTCA-Mn(II)}_2/(\gamma\text{-bilirubin})]^{4+}$ (top), and $[\text{PTTCA-Mn(II)}_2/(\gamma\text{-bilirubin})_2]^{4+}$ complex (down).

complexation of γ -bilirubin with biosensor is of 1:2 stoichiometry, $[\text{PTTCA-Mn(II)}_2/(\gamma\text{-bilirubin})_2]^{4+}$. Therefore, the $[\text{PTTCA-Mn(II)}_2/(\gamma\text{-bilirubin})_2]^{4+}$ complexes have been designed and optimized at three different spin states. To compare energies and some geometrical parameters of all above complexes, Table 7 as well as see Fig. 6 and 7 summarize the B3LYP computed results. The calculated relative stability energy of $[\text{PTTCA-Mn(II)}_2/(\gamma\text{-bilirubin})]^{4+}$ and $[\text{PTTCA-Mn(II)}_2/(\gamma\text{-bilirubin})_2]^{4+}$ complexes illustrate the addition of one γ -bilirubin molecule to the $[\text{PTTCA-Mn(II)}_2/(\gamma\text{-bilirubin})]^{4+}$ complex in high spin state release 99.36 kcal/mol energy, see Fig. 6. In addition, for both 1:1 and 1:2 stoichiometry high spin state is the most stable complex. The relative stability energy for high spin state in $[\text{PTTCA-Mn(II)}_2/(\gamma\text{-bilirubin})_2]^{4+}$ complex is about 22.51 kcal/mol and 30.67 kcal/mol than low and intermediate spin state, respectively. The interacted sites of γ -bilirubin to the Mn4 and Mn5 atoms from biosensor are N26, N27, O43, and O2 (or O3) positions.

Taking into consideration relative stability energy of $[\text{PTTCA-Mn(II)}_2/(\gamma\text{-bilirubin})]^{4+}$ and $[\text{PTTCA-Mn(II)}_2/(\gamma\text{-bilirubin})_2]^{4+}$ complexes, it is observed that all high spin structures are far more stable than similar intermediate and low

QM study of complexation between natural bilirubin and PTTCA-Mn(II)

Table 7. Presentation of some structural details of [PTTCA-Mn(II)₂/(γ -bilirubin)]⁴⁺, and [PTTCA-Mn(II)₂/(γ -bilirubin)₂]⁴⁺ complexes in different spin states.

Connected atoms	[PTTCA-Mn(II) ₂ /(γ -bilirubin)] ⁴⁺			[PTTCA-Mn(II) ₂ /(γ -bilirubin) ₂] ⁴⁺		
	Intermedite			Intermedite		
Bond distance (Å)	High spin	spin	Low spin	High spin	spin	Low spin
Mn4-O2	2.09	2.06	1.94	1.83	1.91	1.87
Mn4-O43	2.01	1.99	2.02	2.04	2.00	2.30
Mn4-N27	2.27	2.21	2.20	2.45	2.41	2.41
Mn4-N26	2.23	2.20	2.28	2.29	2.27	2.40
	Bond angle(°)					
O2-Mn4-O43	122.66	120.69	125.08	126.89	122.90	125.71
O2-Mn4-N27	99.21	90.01	114.81	126.89	132.32	130.23
O2-Mn4-N26	144.92	145.96	138.51	124.72	119.05	120.95
	Dihedral angle(°)					
C1-O2-Mn4-O43	-54.91	-50.05	-45.29	-136.30	135.14	132.71
C1-O2-Mn4-N27	-160.42	-151.79	-174.09	-1.54	-96.22	-95.71
C1-O2-Mn4-N26	118.09	126.13	85.64	98.62	-1.67	94.23

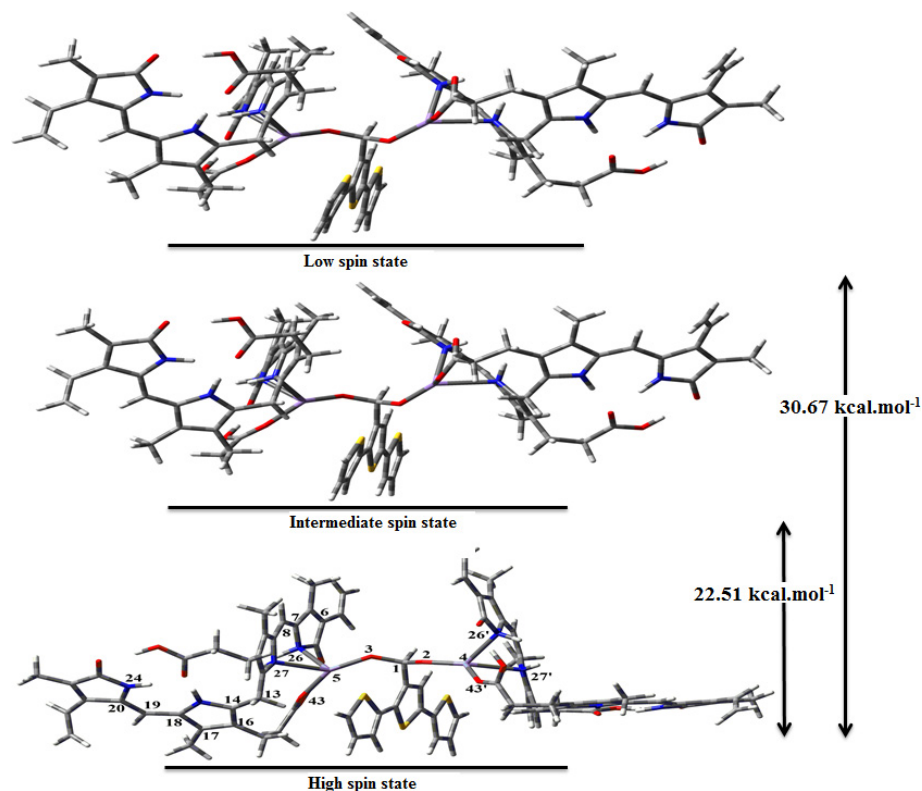


Fig. 7. Computed relative energy for optimized structure of [PTTCA-Mn(II)₂/(γ -bilirubin)₂]⁴⁺ complexes in different spin states with numbering for some key atoms.

M. Ghiasi, M. Molaei & M. Zahedi

spin states. It may be concluded that deformation energy of γ -bilirubin in relative energies in various spin states could affect the stability of these complexes. By taking a look at the structural details of $[\text{PTTCA-Mn(II)}_2/(\gamma\text{-bilirubin})]^{4+}$ and $[\text{PTTCA-Mn(II)}_2/(\gamma\text{-bilirubin})_2]^{4+}$ complexes in different spin states, it reveals that the deformation energy of γ -bilirubin in $[\text{PTTCA-Mn(II)}_2/(\gamma\text{-bilirubin})]^{4+}$ complex is 13.5 and 10.7 kcal/mol and in $[\text{PTTCA-Mn(II)}_2/(\gamma\text{-bilirubin})_2]^{4+}$ complex is 7.5 and 6.5 kcal/mol for low and intermediate spin states, respectively.

3.5. Interaction study between trimer PTTCA-Mn(II) complex, $[\text{PTTCA-Mn(II)}_2]$, and natural γ -bilirubin

To show the effect of PolyTTCA polymer ($-\text{[PTTCA]}_n- \dots -\text{PTTCA-PTTCA-PTTCA}-\dots$) as the supporting material, the $[\text{PTTCA}]_3 = \text{PTTCA-PTTCA-PTTCA}$ model has been used to interact with γ -bilirubin, the most stable isomer of bilirubin. It is noticeable that in this part we just optimized the complexes in high spin state. At first, $[(\text{PTTCA-Mn(II)}_2)_3/(\gamma\text{-bilirubin})_3]^{12+}$ complex (1:1) has been constructed and fully optimized at high spin state. As the calculated results indicate, both Mn^{2+} ions in the biosensor molecule have four-coordinate structure with tetrahedral geometry. The second possible complex of γ -bilirubin with biosensor has 1:2 stoichiometry, $[(\text{PTTCA-Mn(II)}_2)_3/(\gamma\text{-bilirubin})_6]^{12+}$, see Fig. 8. The calculated relative stability energy of $[\text{PTTCA-Mn(II)}_2/(\gamma\text{-bilirubin})]^{4+}$ and $[(\text{PTTCA-Mn(II)}_2)_3/(\gamma\text{-bilirubin})_3]^{12+}$ complexes illustrate that using the three monomer ($-\text{PTTCA-PTTCA-PTTCA}-$) instead of single monomer 51 kcal/mol energy has been released. Also, calculated stability energy related to $[\text{PTTCA-Mn(II)}_2/(\gamma\text{-bilirubin})_2]^{4+}$ and $[(\text{TTCA-Mn(II)}_2)_3/(\gamma\text{-bilirubin})_6]^{12+}$ complexes indicate the

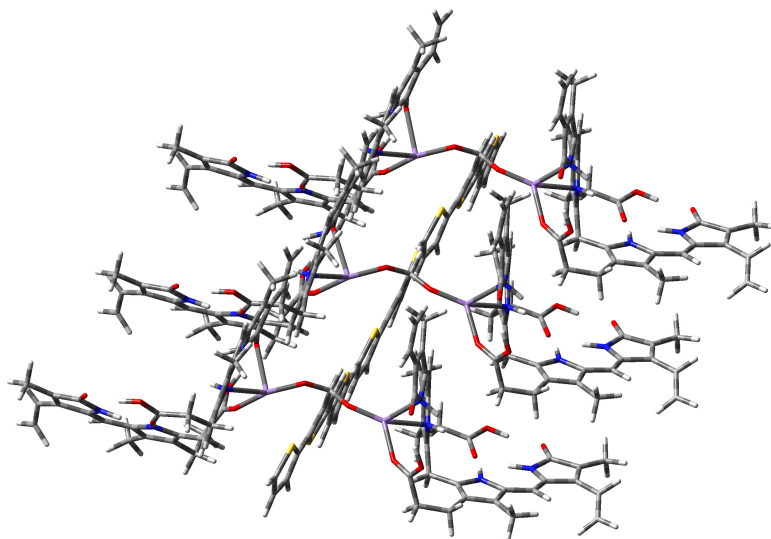


Fig. 8. Optimized structure of $[\text{PTTCA-Mn(II)}_3/(\gamma\text{-bilirubin})_6]^{12+}$ complex.

QM study of complexation between natural bilirubin and PTTCA-Mn(II)

release of 47 kcal/mol energy. In addition, for both 1:1 and 1:2 stoichiometries in high spin state, addition of one monomer (PTTCA) leads to the release of about 16 kcal/mol energy. The calculated relative stability energy of $[(\text{PTTCA-Mn(II)}_2)_3/(\gamma\text{-bilirubin})_3]^{12+}$ complex illustrates that the addition of one γ -bilirubin molecule to the $[\text{PTTCA-Mn(II)}_2/(\gamma\text{-bilirubin})]^{4+}$ complex in high spin state leads to release of 88.5 kcal/mol energy. The coordinated sites of γ -bilirubin in both complexes, $[(\text{PTTCA-Mn(II)}_2)_3/(\gamma\text{-bilirubin})_3]^{12+}$ and $[(\text{PTTCA-Mn(II)}_2)_3/(\gamma\text{-bilirubin})_6]^{12+}$, are the same as the $[\text{PTTCA-Mn(II)}_2/\gamma\text{-bilirubin}]^{4+}$ and $[\text{PTTCA-Mn(II)}_2/(\gamma\text{-bilirubin})_2]^{4+}$ complexes.

3.6. Interference effect

According to previous experimental study,²⁷ the effects of some common interfering bio-compounds such as ascorbic acid, L-glutamic acid, uric acid, creatine, glucose, and dopamine in the determination of bilirubin were evaluated, see Figs. 9 and 10. The experimental results showed that the sensor response was not affected by the presence of L-glutamic acid, uric acid, creatine, and glucose in normal physiological concentration. However, ascorbic acid and dopamine were found to interfere with bilirubin detection which was completely eliminated by coating the polyTTCA-Mn(II) complex electrode with ascorbate oxidase and polyethyleneimine. Therefore, we are interested to show the binding energy calculations of above mentioned interferers with polyTTCA-Mn(II) complex biosensor. To find more suitable atomic sites of interferers to interact with manganese cations in PTTCA-Mn(II)₂ biosensor, the net atomic charges are evaluated. These partial charges are derived from NPA calculation. The more negative charges have been detected on O8 (−0.64), N10

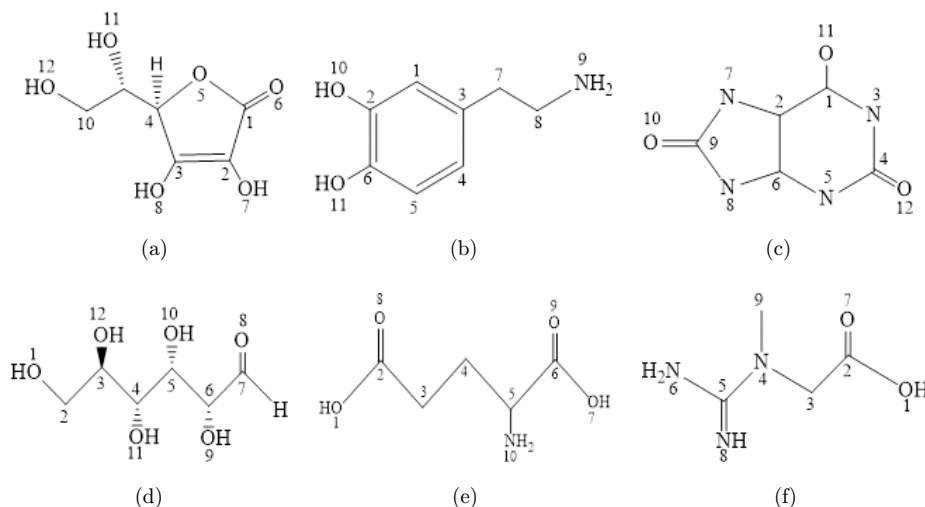


Fig. 9. Schematic representation with numbering of interferers, (a) ascorbic acid, (b) dopamine, (c) uric acid, (d) glucose, (e) glutamic acid, and (f) creatine.

M. Ghiasi, M. Molaei & M. Zahedi

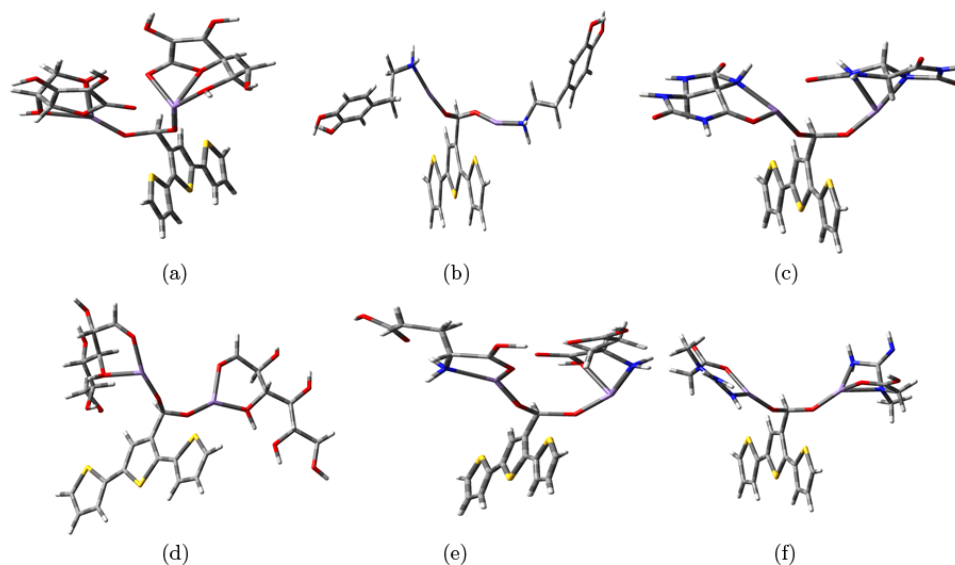


Fig. 10. Optimized structure of different complexes between PTTCA-Mn(II) and interferers, (a) ascorbic acid, (b) dopamine, (c) uric acid, (d) glucose, (e) glutamic acid, and (f) creatine.

(−0.71), N8 (−0.67), N6 (−0.79), O11 (−0.65), and N9 (−0.73) in ascorbic acid, L-glutamic acid, uric acid, creatine, glucose and dopamine, respectively. In conclusion, these atoms are more preferred than other atoms to interact with manganese cations. Figure 10 shows the optimized complex structure between PTTCA-Mn(II)₂ biosensor and different interferers in high spin state. Comparison between γ -bilirubin binding energy in [PTTCA-Mn(II)₂/(γ -bilirubin)₂]⁴⁺ complex (−354.71 kcal/mol) and interferers binding energy, see Table 9, indicates a greater tendency of bilirubin to interact with biosensor. The following binding energy sequence for the six

Table 8. Net atomic charges and spin density of interacting atoms of [PTTCA-Mn(II)₂/(γ -bilirubin)₂]⁴⁺ complex in high spin state.

Atom number	Particle atomic charges	Spin density
Mn(5)	1.08	4.78
Mn(4)	1.08	4.79
N(26)	−0.87	0.01
N(27)	−0.82	0.00
O(2)	−0.71	0.09
O(43)	−0.61	0.01
N(26')	−0.87	0.01
N(27')	−0.82	0.00
O(3)	−0.71	0.08
O(43')	−0.59	0.01

QM study of complexation between natural bilirubin and PTTCA-Mn(II)

Table 9. Comparison of binding energies related to γ -bilirubin and complexes of interfering agents.

Molecule	$\Delta E_{\text{rxn.}}$ (kcal.mol ⁻¹)
	B3LYP/6-31G*
γ -bilirubin	-354.71
Ascorbic acid	-284.81
Dopamine	-240.61
Uric acid	-201.42
Glucose	-246.63
Glutamic acid	-250.06
Creatine	-299.86

interferences and γ -bilirubin is obtained: glutamic acid < uric acid < glucose < dopamine < ascorbic acid < creatine << γ -bilirubin.

3.7. Temperature effect

Experimental results show the effect of temperature to response of biosensor to bilirubin detection in the range of 10–70°C.²⁷ To illustrate the temperature effect on the binding energy of natural bilirubin, the frequency calculations have been run for [PTTCA-Mn(II)₂/(γ -bilirubin)₂]⁴⁺ complex in the range of 10–70°C while $\Delta H_{\text{binding}}^{\circ}$ has been calculated, $\Delta H_{\text{binding}}^{\circ} = [H_{\text{complex}}^{\circ}] - [H_{\text{PTTCA}}^{\circ} + 2H_{\text{bilirubin}}^{\circ}]$. Subsequently, $\Delta E_{\text{binding}}$ has been evaluated according to $\Delta E = \Delta H - \Delta nRT$ equation and reported in Table 10. As the results indicate, three different regions are exhibited. In the first region (10–30°C) the binding energy (binding enthalpy) has been slightly decreased, however, the binding energy (binding enthalpy) rapidly is decreased from 30°C to 60°C, whereas in the third region (60–70°C), the binding enthalpy has not been changed significantly. Our calculated results are in good agreement with experimental results. This high temperature dependency of the bilirubin binding might be related to the temperature related activity of the manganese ion (Mn²⁺) complex.

3.8. Nature of interaction between Mn²⁺ in biosensor and γ -bilirubin

3.8.1. Molecular orbital analysis point of view

To find the nature of binding between bilirubin and Mn²⁺, molecular orbital (MO) analysis has been employed. This analysis is useful to present the factors influencing

Table 10. Evaluation of temperature effect on binding energy in [PTTCA-Mn(II)₂/(γ -bilirubin)₂]⁴⁺ complexes in the range of 10–70°C.

	10°C	20°C	25°C	30°C	40°C	50°C	60°C	70°C
$\Delta E_{\text{binding}}$ (kcal.mol ⁻¹)	-332.15	-343.98	-354.71	-425.43	-475.15	-510.12	-530.75	-531.12
$\Delta H_{\text{binding}}$ (kcal.mol ⁻¹)	-231.14	-342.82	-353.53	-424.23	-473.85	-508.17	-528.95	-530.1

M. Ghiasi, M. Molaei & M. Zahedi

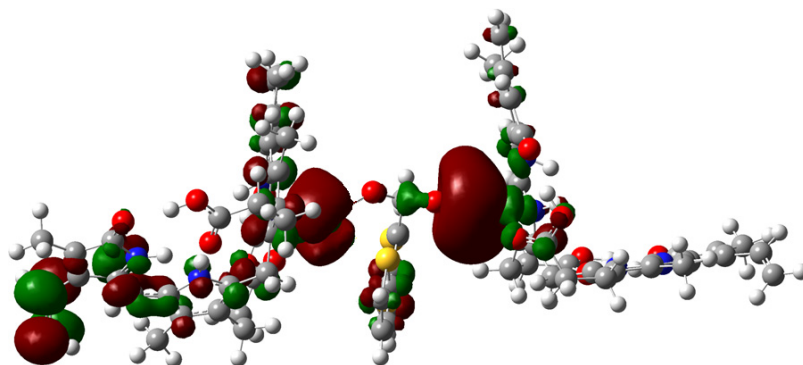


Fig. 11. HMOOs for the $[\text{PTTCA-Mn(II)}_2/(\gamma\text{-bilirubin})_2]^{4+}$ complex at high spin state.

the stability of these kinds of complexes.^{39–41} Taking into account the above discussion, we focused mostly on the $[\text{PTTCA-Mn(II)}_2/(\gamma\text{-bilirubin})_2]^{4+}$ complex in high spin state. Figure 11 depicts the highest mono-occupied orbital (HMOO) of high spin state of $[\text{PTTCA-Mn(II)}_2/(\gamma\text{-bilirubin})_2]^{4+}$ complex. HMOO includes contributions of both Mn^{2+} and interacting heteroatoms of γ -bilirubin. The presented HMOO orbital in Fig. 11 reveals an antibonding interaction between metal ion and ligand orbitals. These antibonding MOs arise from the interaction between $d\sigma$ orbital of the metal and lone pairs of nitrogen atoms in γ -bilirubin.

3.8.2. NPA point of view for $[\text{PTTCA-Mn(II)}_2/(\gamma\text{-bilirubin})_2]^{4+}$ complex in high spin states

Calculated net atomic charges and spin density of $[\text{PTTCA-Mn(II)}_2/(\gamma\text{-bilirubin})_2]^{4+}$ complex in high spin states are presented in Table 8. These partial charges are derived from NPA calculation. The net atomic charge on the Mn4 and Mn5 is about 1.5 and the spin density is almost entirely located on the manganese atoms, 4.79 and 4.78, respectively, when two manganese atoms are coordinated to γ -bilirubin from N26, N27, and O43 positions. By taking into account charge and spin densities of γ -bilirubin interacting atoms, N26 (−0.87, 0.01), N27 (−0.82, 0), and O43 (−0.61, 0.01), an electron shared interaction between bilirubin and Mn^{2+} ions could be evidenced.

3.8.3. AIM analysis point of view

To gain some insight into the nature of binding between Mn^{2+} in biosensor and bilirubin, AIM analysis has been employed. According to AIM theory, each nucleus in a molecule is surrounded by the region called an atomic basin which is bounded by a zero-flux surface in $\nabla^2\rho$ that defines an atomic boundary. When two atoms share some portion of their surfaces, a line of maximum electronic charge density is formed between the nuclei, and at the point where the shared surface interests this atomic interaction line there is a saddle point in $\rho(\mathbf{r})$ called a bond critical point (BCP).⁴² In

QM study of complexation between natural bilirubin and PTTCA-Mn(II)

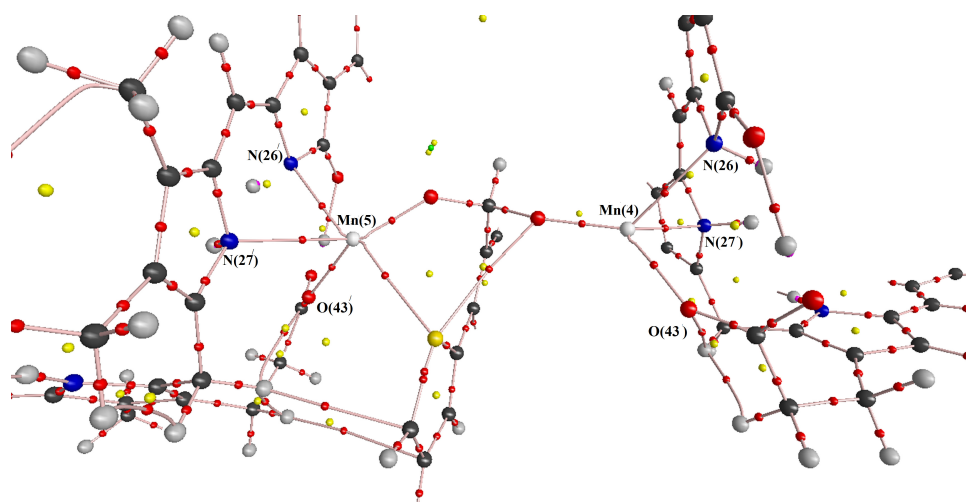


Fig. 12. Molecular graph of $[\text{PTTCA-Mn(II)}_2/(\gamma\text{-bilirubin})_2]^{4+}$ complex showing all BCP and RCP.

this manner, AIM theory identifies a unique line of communication between two chemically interacting nuclei and provides a unique point which can probe or characterize the interaction. The topology of $\rho(\mathbf{r})$ at a BCP is described by the real, symmetric, second rank Hessian of $\rho(\mathbf{r})$ tensor.

The most immediate evidence of bonding within the AIM formalism is the existence of a bond path between two atoms and a BCP in the path. The molecular graph as revealed by the AIM analysis, has been presented in Fig. 12. The path of BCPs for this complex indicated that the bonds between the bilirubin atoms, N and O atoms, and Mn(II) ions have covalent nature. The topological properties such as density and density Laplacian for the $[\text{PTTCA-Mn(II)}_2/(\gamma\text{-bilirubin})_2]^{4+}$ complex are presented in Table 11. The sign of the Laplacian (supposed to be positive for “closed shell interaction” like ionic bonds or hydrogen bonds and unlike covalent bonds) corresponds to this kind of interaction.⁴³

Table 11. Density and density Laplacian at BCPs between Mn^{2+} in biosensor and γ -bilirubin atoms in $[\text{PTTCA-Mn(II)}_2/(\gamma\text{-bilirubin})_2]^{4+}$ complex.

Bond	$100 \times (\rho)$	$100 \times \nabla^2(\rho)$
Mn4–O43'	12.49	–1.13
Mn4–N27'	0.24	–0.01
Mn4–N26'	3.64	–5.80
Mn5–O43	7.81	–8.85
Mn5–N27	14.08	–2631.91
Mn5–N26	972.42	–842.46

M. Ghiasi, M. Molaei & M. Zahedi

4. Conclusion

Quantum mechanical calculations have been performed for reduction processes of natural biliverdin to natural bilirubin. Furthermore, the geometry of PTTCA–Mn(II)₂ biosensor has been optimized in three possible different spin states, low ($S = 1/2$), intermediate ($S = 3/2$) and high spin state ($S = 5/2$). In addition, coordination properties of β -, δ - and γ -bilirubin to both Mn²⁺ ions in biosensor PTTCA–Mn(II)₂ have been studied extensively. Six different complexes including [PTTCA–Mn(II)₂/(δ -bilirubin)₂]⁴⁺, [PTTCA–Mn(II)₂/(β -bilirubin)₂]⁴⁺, [PTTCA–Mn(II)₂/(δ -bilirubin)₂(H₂O)₂]⁴⁺, [PTTCA–Mn(II)₂/(β -bilirubin)₂(H₂O)₂]⁴⁺, [PTTCA–Mn(II)₂/(γ -bilirubin)]⁴⁺, and [PTTCA–Mn(II)₂/(γ -bilirubin)₂]⁴⁺ have been considered in detail to provide a complete picture of minimum energy complex and to assess the ground spin state. The results reveal that the most stable spin states are the high spin state form in all cases. Also, for γ -bilirubin, reduced product from biliverdin in the presence of bilirubin reductase enzyme in physiologic media, the [PTTCA–Mn(II)₂/(γ -bilirubin)₂]⁴⁺ complex (1:2 stoichiometry) rather than [PTTCA–Mn(II)₂/ γ -bilirubin]⁴⁺ complex (1:1 stoichiometry) is more stable in all different spin states. We anticipate that these results are fruitful to develop biosensors which might be potent in the detection of bilirubin in clinical samples.

5. Acknowledgments

The authors gratefully acknowledge the research council of Alzahra University for their financial support. Technical support of the Chemistry Computation Center at Shahid Beheshti University is greatly acknowledged.

References

1. With TK, *Bile Pigments, Chemical Biological and Clinical Aspects*, Academic Press, New York, 1968.
2. Avramescu ME, Sager WFC, Borneman Z, Wessling M, Adsorptive membranes for bilirubin removal, *J Chromatogr B* **803**:215–223, 2004.
3. Wang X, Chowdhury JR, Chowdhury NR, Bilirubin metabolism: Applied physiology, *Curr Pediatr* **16**:70–74, 2004.
4. Miyano Go, Nakamura H, Takahashi T, Lane GJ, Yamataka A, Total bilirubin in nasogastric aspirates: A potential new indicator of postoperative gastrointestinal recovery, *Afr J Paediatr Surg* **10**:243–245, 2013.
5. Zahedi M, Kamalipour M, Safari N, Theoretical studies of biliverdin: Energetics of the reduction pathways to bilirubin, *J Mol Model* **8**:113–118, 2002.
6. Nogales D, Lightner DA, On the structure of bilirubin in solution. 13C [1H] heteronuclear Overhauser effect NMR analyses in aqueous buffer and organic solvents, *J Biol Chem* **270**:73–77, 1995.
7. Boiadjev SE, Lightner DA, An enantiomerically pure bilirubin: Absolute configuration of α R, α' R)-dimethylmesobilirubin-XIII α , *Tetrahedron Asymmetry* **12**:2551–2564, 2001.
8. Person RV, Peterson BR, Lightner DA, Bilirubin conformational-analysis and circular-dichroism, *J Am Chem Soc* **116**:42–59, 1994.

QM study of complexation between natural bilirubin and PTTCA-Mn(II)

9. Shelver WL, Rosenberg H, Shelver WH, Molecular conformation of bilirubin from semiempirical molecular orbital calculations, *Int J Quantum Chem* **44**:141–163, 1992.
10. Dorner T, Knipp B, Lightner DA, Heteronuclear NOE analysis of bilirubin solution conformation and intramolecular hydrogen bonding, *Tetrahedron* **53**:2697–2716, 1997.
11. Shelver WL, Rosenberg H, Semiempirical molecular orbital calculations on the role of hydrogen bonding in the structure of bilirubin dianion, *J Mol Struct (Theochem)* **312**:1–9, 1994.
12. Zahedi M, Ghiasi M, Safari N, Modeling of biliverdin reduction process: Regio-specificity and H-bonding, *Chem Phys* **310**:179–187, 2005.
13. Torben KW, The bilirubin excretion test as a functional liver test with remarks on the course of the curve of the serum bilirubin, *Acta Med Scand CXVI*:96–113, 1943.
14. Piwowska J, Kuczyńska J, Pachecka J, Liquid chromatographic method for the determination of lidocaine and monoethylglycine xylidide in human serum containing various concentrations of bilirubin for the assessment of liver function, *J Chromatogr B* **805**:1–5, 2004.
15. Tiribelli C, Ostrow JD, The molecular basis of bilirubin encephalopathy and toxicity: Report of an EASL Single Topic Conference, *J Hepatol* **43**:156–66, 2005.
16. Winger J, Michelfelder A, Diagnostic Approach to the Patient with Jaundice, *Prim Care, Clin Off Prac* **36**:469–482, 2011.
17. Ostrow JD, *Bile Pigments and Jaundice*, Marcel Dekker, New York, 1986.
18. Almaas A, Hankø E, Mollnes TE, Rootwelt T, Dexamethasone reduces bilirubin-induced toxicity and IL-8 and MCP-1 release in human NT2-N neurons, *Brain Res* **1458**:12–16, 2012.
19. Wang J, Ozsoz MA, Polishable amperometric biosensor for bilirubin, *Electroanalysis* **2**:647–650, 1990.
20. Yang Z, Yan J, Zhang C, Piezoelectric detection of bilirubin based on bilirubin-imprinted titania film electrode, *Anal Biochem* **421**:37–42, 2012.
21. Kurosaka K, Senba S, Tsubota H, Kondo H, A new enzymatic assay for selectively measuring conjugated bilirubin concentration in serum with use of bilirubin oxidase, *Clin Chim Acta* **269**:125–136, 1998.
22. Brandl M, Kellner K, Posniecek T, Bado L, Falkenhagen D, Spectroscopic hemoglobin and bilirubin measurement on optically opaque particulate fluids, *Sens Actuators B* **182**:711–717, 2013.
23. Zelenka J, Leníček M, Muchová L, Jirsa M, Kudla M, Balaž P, Zadinová M, Ostrow JD, Wong RJ, Vitek L, Highly sensitive method for quantitative determination of bilirubin in biological fluids and tissues, *J Chromatogr B* **867**:37–42, 2008.
24. Mullon CJP, Langer RC, Determination of conjugated and total bilirubin in serum of neonates, with use of bilirubin oxidase, *Clin Chem* **33**:1822–1825, 1987.
25. Furtuney A, Guibault GG, Enzyme electrode for the determination of bilirubin, *Electroanalysis* **8**:229–232, 1996.
26. Ponhong K, Teshima N, Grudpan K, Motomizu S, Sakai T, Simultaneous injection effective mixing analysis system for the determination of direct bilirubin in urinary samples, *Talanta* **87**:113–117, 2011.
27. Rahman A Md, Lee KS, Park DS, Won MS, Shim YB, An amperometric bilirubin biosensor based on a conductive poly-terthiophene-Mn(II) complex, *J Biosens Bioelectron* **23**:857–864, 2008.
28. Frisch, MJ, Trucks GW, Schlegel HB, Scuseria GE, Robb MA, Cheeseman JR, Zakrzewski V, Montgomery JA, Stratmann RE, Burant JC, Dapprich S, Millam JM, Daniels AD, Kudin KN, Strain MC, Farkas O, Tomasi J, Barone V, Cossi M, Cammi R, Mennucci B, Pomelli C, Adamo C, Clifford S, Ochterski J, Petersson GA, Ayala PY, Cui Q, Morokuma K, Malick DK, Rabuck AD, Raghavachari K, Foresman JB, Cioslowski J,

M. Ghiasi, M. Molaei & M. Zahedi

- Ortiz JV, Stefanov BB, Liu G, Liashenko A, Piskorz P, Komaromi I, Gomperts R, Martin RL, Fox DJ, Keith T, Al-Laham MA, Peng CY, Nanayakkara A, Gonzalez C, Challacombe M, Gill PMW, Johnson BG, Chen W, Wong MW, Andres JL, Head-Gordon M, Replogle ES, Pople JA, Gaussian 98 (Revision A.1), Gaussian, Inc., Pittsburgh PA, 2003.
29. Beck ADJ, Density-functional thermochemistry III: The role of exact exchange, *Chem Phys* **98**:5648–5652, 1993.
 30. Parr RG, Yang W, *Density-functional theory of atoms and molecules*, Oxford University Press, Oxford, 1989.
 31. Wong MW, Frisch MJ, Wiberg KB, Solvent Effects 3. Tautomeric Equilibria of Formamide and 2-Pyridone in the Gas Phase and Solution: An *ab Initio* SCRF Study, *J Am Chem Soc* **114**:1645–1652, 1992.
 32. Petersson GA, Al-Laham MA, A complete basis set model chemistry II: Open-shell systems and the total energies of the first-row atoms, *J Chem Phys* **94**:6081–6090, 1991.
 33. Wong MW, Gill PMW, Nobes RH, 6-311G(MC)(d,p): A second-row analogue of the 6-311G(d,p) basis set: Calculated heats of formation for second-row hydrides, *J Phys Chem* **92**:4875–4880, 1988.
 34. Frisch MJ, Carpenter JE, *The Structure of Small Molecules and Ions*, Plenum, New York, 1988.
 35. Bader RFW, *Atoms in Molecules: A Quantum Theory*, Oxford Science Publication, Clarendon Press, London, 1990.
 36. Khodabandeh MH, Davari M, Zahedi M, Ohanessian G, Complexation of glycine by manganese(II) in the gas phase: A theoretical study, *Int J Mass Spectrom* **291**:73–83, 2010.
 37. Khodabandeh, MH, Reisi H, Davari M, Zare K, Zahedi M, Ohanessian G, Interaction modes and absolute affinities of α -amino acids for Mn^{2+} : A comprehensive picture, *ChemPhysChem* **00**:1–14, 2013.
 38. Avelino de Abreu H, Guimaraes L, Duarte HA, DFT/PCM Investigation of the Mn(II) chemical speciation in aqueous solution, *Int J Quantum Chem* **108**:2467–2475, 2008.
 39. Bertran J, Rodriguez-Santiago L, Sodupe M, Density functional cluster model study of bonding and coordination modes of CO_2 on Pd (1 1 1). *Surf Sci* **431**:208–219, 1999.
 40. Rogalewicz F, Ohanessian G, Gresh N, Interaction of neutral and zwitterionic glycine with Zn^{2+} in gas phase: *ab initio* and SIBFA molecular mechanics calculations, *J Comput Chem* **21**:963–973, 2000.
 41. Rodriguez-Santiago L, Sodupe M, Gas-phase reactivity of Ni^+ with glycine, *J Phys Chem A* **105**:5340–5347, 2001.
 42. Cremer D, Kraka E, Slee TS, Bader RFW, Lau CDH, Nguyen-Dang TT, MacDougall PJ, Description of homoaromaticity in terms of electron distributions, *J Am Chem Soc* **105**:5069–5075, 1983.
 43. Koch U, Popelier PLA, Characterization of C–H–O Hydrogen bonds on the basis of the charge density, *J Phys Chem* **99**:9747–9754, 1995.